Investigo
Universidade Vigo

Biblioteca Universitaria
Área de Repositorio Institucional

Accepted Manuscript

This is the peer reviewed version of the following article which has been published in final form at https://doi.org/10.1002/admt.202202104

Please cite this article as:

M. Maia, A. L. Pires, M. Rocha, S. Ferreira-Teixeira, P. Robalinho, O. Frazão, C. Furtado, A. Califórnia, V. Machado, S. Bogas, C. Ferreira, J. Machado, L. Sousa, U. G. Luis, A. M. G. San-Juan, P. O. Crespo, F. N. Medina, C. U. Sande, A. C. Marino, G. R. González, A. T. Pereira, F. A. Agelet, R. Jamier, P. Roy, B. Leconte, J.-L. Auguste, A. M. Pereira, A Photo-Thermoelectric Twist to Wireless Energy Transfer: Radial Flexible Thermoelectric Device Powered by a High-Power Laser Beam. Adv. Mater. Technol. 2023, 8, 2202104. 10.1002/admt.202202104

General rights:

This article may be used for non-commercial purposes in accordance with Wiley Terms and Conditions for Use of Self-Archived Versions. This article may not be enhanced, enriched, or otherwise transformed into a derivative work, without express permission from Wiley or by statutory rights under applicable legislation. Copyright notices must not be removed, obscured, or modified. The article must be linked to Wiley's version of record on Wiley Online Library and any embedding, framing or otherwise making available the article or pages thereof by third parties from platforms, services, and websites other than Wiley Online Library must be prohibited.

A Photothermoelectric Twist to Wireless Energy Transfer: Radial Flexible Thermoelectric Device Powered by a High-Power Laser Beam

M. Margarida Maia, Ana L. Pires, Mariana Rocha, Sofia Ferreira-Teixeira, Paulo Robalinho, Orlando Frazão, Cristina Furtado, António Califórnia, Vasco Machado, Sarah Bogas, César Ferreira, João Machado, Luís Sousa, Uxía L. García, Alejandro G. Sanjuan, Pedro O. Crespo, Fermin N. Medina, Carlos U. Sande, Alejandro G. Camanzo, Guillermo R. González, Fernando A. Agelet, Raphael Jamier, Philippe Roy, Baptiste Leconte, Jean-Louis Auguste, André M. Pereira**

M. M. Maia, A. L. Pires, M. Rocha, S. Ferreira-Teixeira, A. M. Pereira
IFIMUP – Institute of Physics for Advanced Materials, Nanotechnology and Photonics,
Department of Physics and Astronomy,
Faculty of Sciences of the University of Porto, Porto, Portugal.
E-mail: ana.pires@fc.up.pt, ampereira@fc.up.pt

P. Robalinho, O. Frazão
INESC-TEC
R. Dr. Roberto Frias, Porto, Portugal

C. Furtado, A. Califórnia, V. Machado, S. Bogas, C. Ferreira, J. Machado, L. Sousa
CeNTI - Centre for Nanotechnology and Smart Materials
R. Fernando Mesquita, Vila Nova de Famalicão, Portugal.

U. L. García, A. G. Sanjuan, P. O. Crespo, F. N. Medina, C. U. Sande, A. G. Camanzo, G. R. González, F. A. Agelet
University of Vigo,
Vigo (Pontevedra), 36310, Spain.

R. Jamier, P. Roy, B. Leconte, J.-L. Auguste
XLIM Research Institute
123, avenue Albert Thomas, Limoges Cedex, 87060, France.

Keywords: wireless energy transfer, thermoelectric devices, high-power lasers, screen-printing, space exploration

Wireless energy transfer (WET) systems are becoming increasingly appealing nowadays. Herein, we present a WET system based on the photothermoelectric effect (PTE). With an incident laser beam at λ=1450 nm, a temperature gradient is generated in the radial flexible thermoelectric (TE) device, with a carbon-based light collector in its center to enhance the photo-heating. The 3-part prototype presents a unique approach by using a radial TE device with one simple manufacturing process – screen-printing. A TE ink with a polymeric matrix of PEDOT:PSS and doped-PVA and Sb-Bi-Te (SBT) microparticles was developed, with S~33 μVK^{-1} and σ~10.31 Sm^{-1}, presenting good mechanical and electrical stability. Regarding the device, a full electrical analysis was performed, and the influence of the light collector was studied using thermal tests, spectrophotometer measurements and numerical simulations. A maximum output voltage of ~16 mV and a maximum power density of ~25 μWm^{-2} were achieved with a P_{laser}=2 W. Moreover, the device viability under extreme conditions was explored. At T~180 K, a 25% increase in the output voltage compared to room-temperature conditions was achieved, and at low pressures (P~10^{-6} Torr), an increase of 230% was obtained. Overall, the presented prototype allows the supply of energy at long distances, ideal for sensors in remote places, especially for space exploration.

1. Introduction

Over the last few decades, our society has been witnessing the fast-growing interconnected environment responsible for the extraordinary volume of data available. Permanent monitoring is only possible due to the intense network of sensors that allows a broad collection of data. Usually, their implementation relies on the use of batteries, thus requiring maintenance and limiting their lifetime.[1,2]

Hybrid photothermoelectric (PTE) devices are an emerging technology with promising potential for a vast range of applications, mainly for those where the conventional energy supply systems fall short. These devices not only use the thermoelectric (TE) effect (direct conversion of a temperature gradient into a voltage), but can also rely on high light absorption and/or plasmonic phenomena, capable of enhancing the overall generated temperature gradient.[3,4] When that approach is not feasible and higher temperatures are desired, a separated light absorbing system is implemented in a TE generator. That way, the light is focused on the absorber, and the heat is conducted to one of the extremities of the TE part, increasing the temperature of the hot side.[3,5,6] Since the light collector can be tailored and optimized for a specific wavelength, its efficiency can be higher for that radiation, overlooking the efficiency for the whole spectrum. Some examples of these light collectors include simple high light absorbing materials[7,8], layered structures[9,10], dispersions[5,11,12], superlattices[6] and metamaterials and metasurfaces[13–15]. Since some of the studies focus on the implementation of the absorbing materials to the thermoelectric device, their influence is evaluated in commercial thermoelectric generators (TEGs).[13,15] To achieve higher TE performances, previous studies with PTE devices report different techniques to fabricate the TE generators. Some of them include thin-films by photo-lithography[7,8,16], nano dispersions[3,9], and some printing processes such as dispenser printing[6] and drop-casting[12,17]. In particular, Wen *et al.*[5] reports a flexible hybrid photothermoelectric generator composed of a thermoelectric generator and a light-to-thermal conversion layer, with an absorbing and a reflective sides. Although the TEG is produced by screen-printing, the light-to-thermal conversion layer is fabricated by blade coating, making it more difficult to transfer to mass production. Furthermore, the proposed device reached a maximum temperature gradient of 50 K with a simulated sunlight. Due to the linear serpentine design, a large area has to be illuminated, thus decreasing the effective energy to absorb because of the light scattering. In contrast, the radial configuration takes advantage of a small central area where the light can be concentrated in one spot, reducing the illuminated area, increasing the effective absorbed energy for higher temperature gradients. This configuration is more commonly used for cylindrical heat sources, such as conduit pipes[18] and

radioisotopes[19]. Due to the different light sources, configurations, and operation conditions, a direct comparison between the various devices described in the literature is not yet possible, but the fast evolution of these technologies appear promising.

In the improvement of the overall performance of a PTE, the thermoelectric component plays a significant role. Bi-Te alloys are the most conventional materials used to fabricate TE devices due to their excellent performance, especially at low- to room-temperature.[20–22] Despite their high efficiencies in bulk, the lack of versatility and adaptability are challenges to be overcome.[23] For this reason, alternative strategies to apply other types of materials to TE devices are emerging. One of those strategies involves organic materials due to their mechanical flexibility, low-cost fabrication, and low weight.[24–26] For this purpose, the study of several possible organic polymers has increased: conductive polymers[27], such as poly(3,4- ethylene dioxythiophene):poly(styrene sulfonate) (PEDOT:PSS)[28–30], polyaniline (PANI)[31,32], and polypyrrole (PPy)[33,34], that usually present low thermal conductivity; and insulating polymers, such as polyvinylidene fluoride (PVDF)[35,36], epoxy resin[37,38], polylactic acid (PLA)[39,40], polyvinyl pyrrolidone (PVP)[41,42] and polyvinyl alcohol (PVA)[43–45], used as the matrix for inorganic materials, increasing their adhesion.[46] Consequently, the organic composites of Bi-Te alloys appear as a viable approach to combine the high efficiencies of the TE material with the range of possibilities that the flexibility and low cost of the organic polymers can bring.

In particular, Pires *et al.*[44] and Zhang *et al.*[45] show that the use of a PVA and a PEDOT:PSS+PVA matrix with Bi_2Te_3 and $Bi_{0.5}Sb_{1.5}Te_3$, respectively, grants low-cost TE materials with excellent flexibility, with an attractive performance. Likewise, fabricated by screen-printing, the micro-composite of Bi_2Te_3+PVA shows a Power Factor (PF) of 0.4 $\mu WK^{-1}m^{-1}$ with a Seebeck coefficient of -160 μVK^{-1} [44]. Moreover, by using a nano-composite with nanocrystals of $Bi_{0.5}Sb_{1.5}Te_3$ with a PEDOT:PSS+PVA matrix, the developed self-standing TE film, fabricated by drop-casting, shows a higher PF of 47.7 $\mu WK^{-1}m^{-1}$, with an remarkable flexibility.[45]

These Energy Harvesting (EH) systems combined with Wireless Energy Transfer (WET) opens the possibilities of powering devices whilst taking advantage of the prolonged lifetime of these mechanisms due to the conversion of ambient energy, enabling a possible perpetual operation.[47] Due to the advantages of these hybrid devices, their use in systems for energy supply at remote places becomes appealing. In particular, space exploration is highly dependent on solar and radioisotope energy, thus reliable alternatives or complementary systems are appealing to apply in these extreme conditions (low temperature and low pressure).

Overall, WET systems are emerging at a fast rate due to the great necessity to find a solution for the limitations in flexibility, adaptability, convenience and safety that the conventional power transmission operations present. Consequently, numerous WET mechanisms have been developed to replace metal wires/cables in applications where mobility is key.[48] These mechanisms comprise electromagnetic induction, magnetic resonance, and radiofrequency waves, being categorized into nonradiative or radiative. The nonradiative technologies are based on near-field inductive coupling or magnetic resonant coupling, presenting high efficiencies, though highly dependent on the distance, limiting its usage to short and mid-range distances.[49] On the other hand, the radiative mechanisms use antennas or other transmitters to propagate the power waves, allowing the coverage of significant distances (several meters to kilometres). The radiation transmission should be directed to the desired location to achieve high efficiencies, thus relying on tracking mechanisms to detect the desired position.[50] Microwaves and laser beams are well-known forms of electromagnetic radiation used in far-field WET systems.[51] Although microwaves are less affected by atmospheric attenuation, they tend to present safety concerns due to their large wavelengths, which are difficult to collimate, and expensive production making their miniaturization challenging. Contrarily, laser-beam power allows the use of a collimated light beam with a controlled wavelength and direction, with easy integration and volume production, without detrimental interference to electronic devices. Hence, laser-beam power transmission has become an appealing technology in the WET field, especially when coupled with other systems.[52] Lately, laser WET is being combined with photovoltaic cells to power devices at long distances, specifically for space exploration.[53,54] The use of a laser beam over the conventional solar radiation allows the remote illumination of the photovoltaic cells when the solar exposition is insufficient, thus reducing the reliance on energy storage.[55] Another method to take advantage of the high power of a laser beam, besides the photoelectric effect, is related to the concept of EH, particularly the thermoelectric effect, that could be appealing for the laser beam WET systems because it can convert the heat load caused by the incidence of the light into electrical energy. Usually, two main approaches can be considered, *i.e.*, PTE devices as photodetectors[13], and PTE generators for low-power consumption sensors.[7] Due to the low generated thermoelectric voltage, the photodetectors route tends to be more common.[13,14,56] For this reason, and due to the difficulty in having a uniform temperature gradient in environment scenarios for energy harvesting[3], the research in PTE devices has been focused in high efficiencies for the sun light spectrum, *i.e.* visible and near infrared radiation.[5,7,57] However, with the growing development of low-consumption electronics, the generated voltages of a TE generator are becoming more and more

appealing.[58] By reducing the dependence on environment conditions, higher outputs can be achieved. In the case of the PTE effect, a controlled light source can be the key to optimize these devices, thus using sun light is not the most beneficial scenario. Moreover, when using sun light, typically an optical system has to be taken into consideration, *i.e.* a set of lenses to focus the sun rays in the light collector.[8,16] For example, using a collimated coherent light source with a high brightness and at a specific wavelength, *i.e.*, a laser beam, can reduce the complexity of the optical system, as well as, increase the generated heat. In particular, laser beam emission in the near-infrared region (NIR) (λ ~1550 nm), have been used in deep-space optical communications, due to the low atmospheric absorption of the radiation at this wavelength.[59]

In this work, we present a wireless energy transfer system based on flexible radial photothermoelectric devices, where a light beam is focused in the small centre of the device (collector). A controlled high-power laser beam was used to heat the radial thermoelectric device, being focused on a carbon-based light collector, with high absorption at the used wavelength (λ = 1450 nm). This is the first radial PTE for WET in the NIR range, manufactured only by screen-printing. The TE ink was developed by combining Sb-Bi-Te (SBT) microparticles with PEDOT:PSS and doped PVA. The performance of the device was evaluated for different pressures and temperatures to study its viability under extreme conditions for remote applications, mainly space exploration.

2. Results and discussion

2.1. Thermoelectric materials and light collector

2.1.1. Thermoelectric materials

The TE inks developed in this work were obtained by the combination of three different compounds: an inorganic material, a conductive polymer and an insulating polymer, i.e. SBT microparticles, PEDOT:PSS and PVA doped with H_3PO_4, respectively. To have a better understanding of the influence of each component morphologic, structural, and electric transport characterizations were carried out.

The SEM micrographs for the SBT microparticles and the SBT printed film are presented in **Figure 1**.

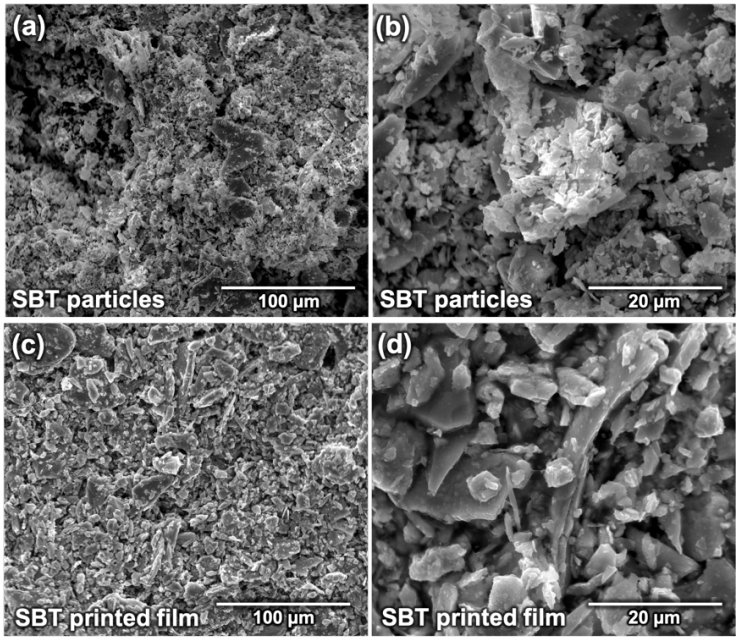

Figure 1 SEM images of a,b. the SBT particles, and c,d. top surface of the SBT printed film, with a magnification of 1 000× and 5 000×, respectively.

The particle size and shape distributions in both samples present a large range, with countless shapes (see **Figure 1a** and **c)**. However, the particles in the printed film appear to be uniformly distributed in size (see **Figure 1b** and **d**). This aspect comes from the high homogeneity of the produced ink and the printing process that allows the even spread of the microparticles. Moreover, the SEM images show the vast distribution of particles along the film, revealing a high density with lower porosity. This fact can be explained by the affinity between the used materials, allowing a uniform ink with high printability qualities for screen-printing (see **Figure 1c)**. The thickness of the sample was determined using the cross-section image (see in **Figure S1** in the Supporting Information), and the value of 53±3 µm was obtained.

From EDS analysis, the atomic percentage of Sb, Bi, and Te for SBT particles and TE film was determined, and it is summarized in **Table S1** in the Supporting Information. The obtained ternary compound presents a majority atomic percentage of Tellurium (Te) (58.3 at%), followed by Antimony (Sb) (28.6 at%), and lastly Bismuth (Bi) (12.0 at%). The stoichiometry of the TE microparticles was determined, thus the resulting powder revealed to be $Sb_{1.47}Bi_{0.62}Te_3$. In the obtained stoichiometry, a combination of an SBT alloy with excess Bi can be seen, differing from the typical $Sb_{2-x}Bi_xTe_3$ compositions.[60–62] Therefore, the studied composite can be identified as $Sb_{1.47}Bi_{0.53}Te_3$ + 1.77 at% Bi. By comparing the atomic percentage of each element, both samples show approximately the same values, thus the combination with the polymeric matrix did not alter the composition of the inorganic particles.

X-ray Diffraction (XRD) analysis was carried out for the different involved compounds, as well as, for the obtained TE film (PEDOT:PSS + doped PVA+ SBT), to inspect the influence of the organic and inorganic materials in the crystallinity of the final printed film. The Kapton substrate, chemically treated as described in the experimental section, was also inspected. **Figure 2** shows the X-ray diffractograms for the different samples (Kapton substrate, PEDOT:PSS (film), doped PVA (film), SBT particles, and SBT printed film) in a range of 2θ = 20º – 80º.

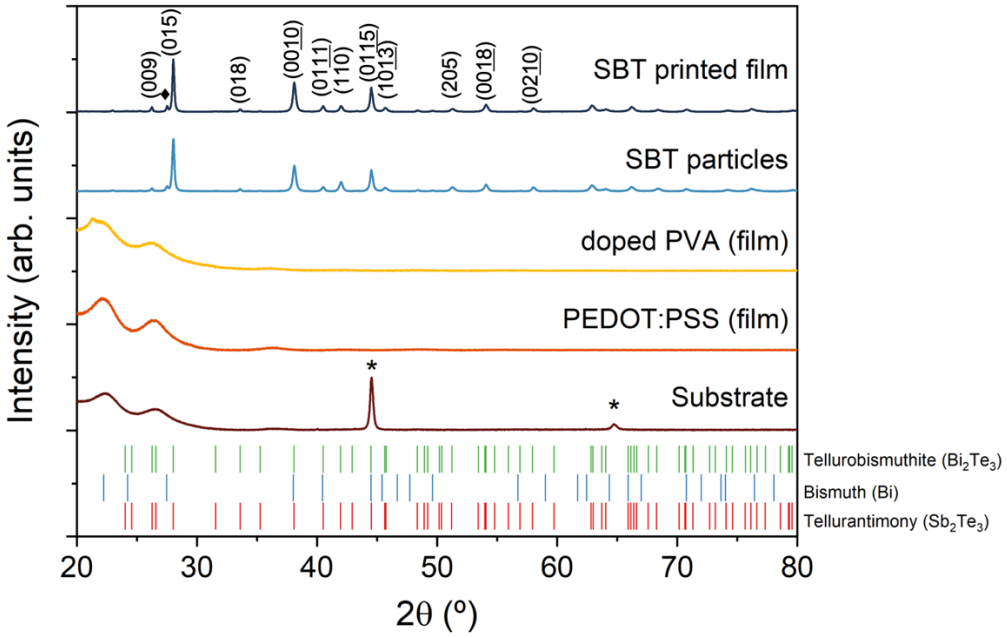

Figure 2 XRD patterns of the different involved compounds, as well as, the TE film (PEDOT:PSS + doped PVA + SBT). The position of the main reflections of Tellurobismuthite (Bi_2Te_3) (JCPDS no. 89-2009), Bismuth (Bi) (JCPDS no. 44-1246), and Tellurantimony (Sb_2Te_3) (JCPDS no. 71-0393) are presented. The main reflections that are identified and indexed correspond to the Tellurantimony (Sb_2Te_3), similar to Tellurobismuthite (Bi_2Te_3). The doped PVA (film) and PEDOT:PSS (film) samples are printed films of the polymers in the substrate. The highlighted reflections (*) correspond to the main Al reflections due to the measurement apparatus. The secondary highlighted reflection (♦) correspond to a Bi main reflection (012), due to the excess of Bi in the SBT particles.

Firstly, regarding the organic compounds, the diffractogram of the substrate presents two crystalline reflections (2θ ~ 44.55º and 2θ ~ 64.78º). These reflections are in concordance with the XRD pattern of aluminum (Al) (as JCPDS 71-1123) and are present due to the sample holder of measuring apparatus. Moreover, the diffractograms for the doped PVA and PEDOT:PSS

films only have present the substrate contribution. This could be due to the low thickness of the printed films, causing a low signal, thus the amorphous envelope is prevalent.[63]

Looking at the inorganic materials, the SBT particles present main reflections that correspond to the Tellurantimony (Sb_2Te_3), similar to Tellurobismuthite (Bi_2Te_3) ($R\bar{3}m$ space group), namely, 2θ = 26.25º (0 0 9), 2θ = 28.03º (0 1 5), 2θ = 33.59º (0 1 8), 2θ = 38.09º (1 0 10), 2θ = 40.52º (0 1 11), 2θ = 41.98º (1 1 0), 2θ = 44.52º (0 1 15), and 2θ = 45.67º (1 0 13). Comparing the lattice parameters, values of a = 4.290(3) Å; c = 30.453(12) Å were obtained, corresponding to the JCPDS no. 71-0393 (Sb_2Te_3) (a = 4.2962 Å; c = 30.4847 Å). The secondary reflection at 2θ = 27.51º (0 1 2) seems to be in agreement with the Bismuth (Bi) pattern. These results match the analysis of SEM/EDS, where an excess Bi was detected. Considering the film's diffractogram, it is evident that the SBT particles are predominant, thus the polymeric matrix does not present any influence in the crystallinity of the printed film, as expected.

Regarding the transport properties, both the SBT particles and the TE film were evaluated.

The SBT microparticles (p-type) present a Seebeck coefficient of +168 μVK^{-1}, and an electrical conductivity of 2379.05 Sm^{-1}, leading to a power factor ($PF = S^2\sigma$) of 67.15 $\mu Wm^{-1}K^{-2}$. These results fit the common TE parameters, but for this specific stoichiometry ($Sb_{1.47}Bi_{0.53}Te_3$), both the electrical conductivity and the Seebeck coefficient present lower values that the ones reported in literature ($\sigma \sim 6000$ Sm^{-1}; $S \sim 220$ μVK^{-1} [64,65]) . The drastic change of the σ value arises from the presence of the excess Bi that increases the Bi_{Te} antisite defects, *i.e.*, the number of charge carriers is reduced, thus decreasing the electrical conductivity.[66] Another, and probably the main, contributing factor for the low value of σ is the low charge mobility in the boundaries of the particles in the pellet produced for the measurement. Due to the irregular shapes of the particles, electron scattering between the boundaries may occur, creating points of high resistance, reducing the overall electrical conductivity of the sample.[44]

Concerning the TE film, after the mixture with the polymeric matrix (SBT + PEDOT:PSS + doped PVA), a decrease in these properties was observed, *i.e.,* S ~33 μVK^{-1} and σ – 10.31 Sm^{-1}, with corresponding PF of 7.97 $nWm^{-1}K^{-2}$. The reduced Seebeck coefficient comes from the relatively high concentration of PEDOT:PSS with low S ($S \sim 13.13$ μVK^{-1})[67], causing a small percolation through the polymer and not the TE particles. Moreover, bending tests were performed to analyze the mechanical performance of the printed film (see **Figure 3**). The results how that with consecutive bending cycles (around 50 cycles) over 275 s, the resistance of the printed film did not present considerable variations, being less than 1%, and maintaining the initial R after the test. Furthermore, the resistance was evaluated for different displacements, thus different bending angles, and slight variations were observed (~ 0.6%). Through these tests,

the Young's Modulus of the printed film on the Kapton substrate was obtained, with a value of 0.64 GPa (see **Figure S2** in Supporting Information). These tests reveal the high mechanical integrity of the printed film, in which its flexibility will not drastically affect the performance of the material.

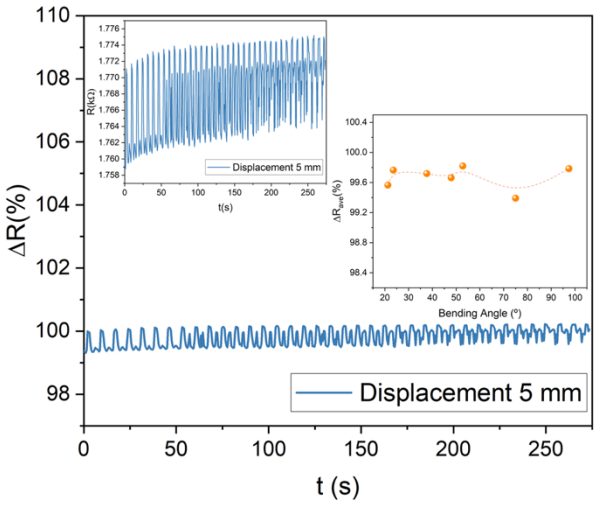

Figure 3 Bending test results, in particular the variation of R (ΔR (%)) during the measurement over 275 s, with a displacement of 5 mm. In inset on the left, the absolute value of R is presented over time during the test. In inset on the right, the average resistance variation (ΔR_{ave} (%)) is shown as a function of the bending angle, obtained for different displacement values.

To study the TE performance under extreme conditions (low temperature), the evaluation of the temperature dependence (20 K – 325 K) of S and σ of the TE film was carried out following Ferreira-Teixeira *et al.* procedure[68]. The results are shown in **Figure 4**.

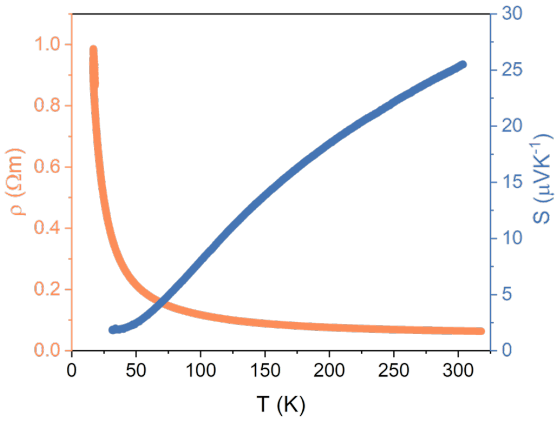

Figure 4 Electrical resistivity (ρ) and Seebeck coefficient (S) of the fabricated TE film as functions of the temperature.

The obtained behavior for the Seebeck coefficient is consistent with the one expected for an organic semiconductor.[69] This is caused by the excessive influence of the PEDOT:PSS causing the percolation, as previously mentioned. The electrical resistivity displays a semiconductor-like behavior, reaching a stable value of ~ 0.14 Ωm after 150 K, that correspond to the electrical conductivity value measured at room temperature (σ ~ 10.31 Sm^{-1}).

Despite presenting lower thermoelectric performance, the developed TE film exhibits good adhesion to the substrate, with high electrical and mechanical stability. For these reasons, the radial flexible TE device was fabricated with this developed ink.

2.1.2. Light absorption materials

To increase the obtained temperature gradient (ΔT) in the TE device, a light absorber material was analyzed, *i.e.*, a commercial carbon-based ink. Hence, a thick film of the carbon-based ink (5 cm x 5 cm) was fabricated by screen-printing in a Kapton substrate, with a thickness of around 22 μm. A comparative thermal analysis between the Kapton substrate (thickness ~75 μm) and the collector film was performed under a continuous-wave (CW) laser beam with a wavelength of 1450 nm in a range of powers from 0 to 1.5 W. In **Figure 5a**, the ΔT values determined for Kapton and the carbon thick film are presented. These values were obtained by directly measuring the temperature at 3 mm and 7 mm from the focusing point with two thermocouples, thus assessing the temperature gradient across the length of a TE stripe in the device.

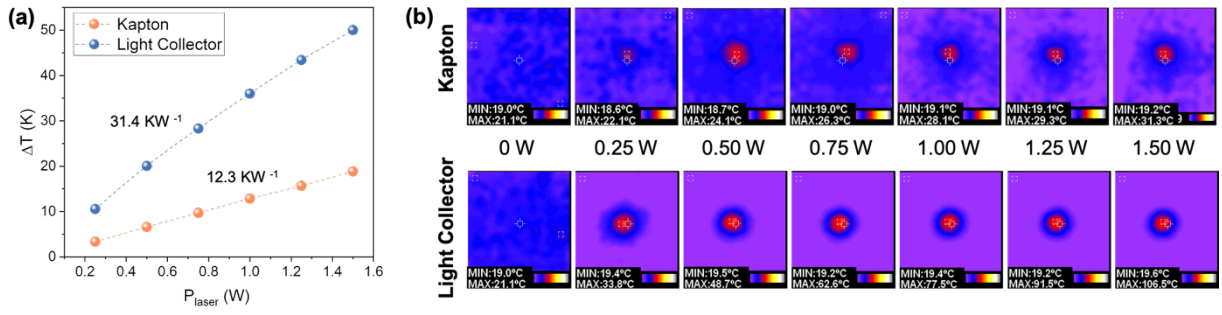

Figure 5 a. Temperature gradient values obtained by measuring the laser heating with thermopowers placed at 3 mm and 10 mm from the focusing point. b. Representative thermal images with an incident laser beam in Kapton and Kapton with the printed light collector, for different values of the laser power values (0 - 1.5 W). The images were captured using Welight® Thermal Pro Infrared camera.

A direct linearity between the laser power and the temperature gradient is verified in both samples, with different rates. The Kapton substrate presents a heating rate of 12.34 KW^{-1}, whilst the collector film has a rate of 31.4 KW^{-1}, more than double the substrate. Hence, a ΔT of ~25 K and ~62 K are expected for a laser power of 2 W, for the Kapton substrate and the collector film, respectively. **Figure 5b** shows the representative thermal images obtained during the tests. These images display the uniform radial heating of the two studied samples. With the light collector, higher temperatures are detected at a given laser power, when compared with the Kapton substrate.

To compare the optical response of the substrate and the light collector, the absorbance of each material was measured for a range of wavelengths from 200 nm to 2000 nm. From the results (see **Figure 6**), the absorbance of Kapton for low wavelengths (< 500 nm) is almost as high as the value for the light collector. Above 500 nm, the absorption decreases drastically, since Kapton is semi-transparent to visible radiation. On the contrary, the light collector film presents a nearly constant absorbance across the whole spectrum, being an opaque material. For our working wavelength (1450 nm; traced line in **Figure 6**), it is evident that the light collector film presents a higher absorption than the substrate, thus a higher temperature can be generated with the incidence of a laser beam with that wavelength.

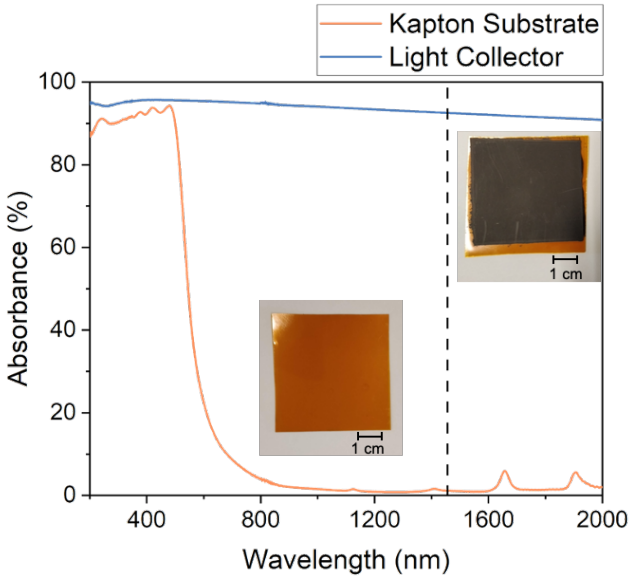

Figure 6 Absorbance of the 75 µm-thick Kapton substrate and the light collector thick film, for a wavelength range from 200 to 2000 nm. The traced line is the 1450 nm wavelength, i.e., the wavelength of the used laser beam. In inset, photos of the two measured samples are presented.

2.1.3. Numerical Simulations

To further verify the different generated ΔT by an incident laser beam in the two considered materials, numerical simulations were carried out using the finite element method on COMSOL Multiphysics. In Supporting Information, the main parameters used in the simulation are presented in detail in **Table S2**. The simulated laser beam has the characteristics of the one used in this study. The properties of the Kapton substrate were used from the native COMSOL database. Because the properties of the carbon-based ink were not all well-known, an estimative with the shooting method was used, namely for the heat capacity (C_p), density (ρ), electrical permittivity ($\varepsilon = \varepsilon' + i\varepsilon''$). The obtained values of C_p and ρ, 1470 $JKg^{-1}K^{-1}$ and 1190 Kgm^{-3}, respectively, are in the same order of magnitude of the ones reported for carbon materials (C_p = 720 $JKg^{-1}K^{-1}$ [70]; ρ = 1700 Kgm^{-3} [71]). The slight discrepancies can be attributed to the polymeric matrix and solvents present in the commercial ink, besides the carbon material.

In **Figure 7a**, the simulated temperature gradients for the substrate and the light collector, with a 2 W CW gaussian laser beam, are presented. Maximum values of $\Delta T \sim 60$ K and $\Delta T \sim 80$ K were obtained for the substrate and the light collector, respectively. The determined values are higher than the one obtained experimentally, *i.e.*, $\Delta T_{Kapton} \sim 25$ K and $\Delta T_{Light\ Collector} \sim 62$ K. The optimum conditions of the simulation and the small deviations of the estimated parameters can explain the slight discrepancies of these values in relation to the experimental data. However, due to the significant difference between the temperatures for the two materials, the results can still demonstrate the viability of the generation of a temperature gradient by an incident laser beam, with an enhancement when a light collector is used. Furthermore, the temperature distribution on the simulated structure appears radial and uniform, thus in concordance with the expected behavior, and advantageous for the chosen device design (see **Figure 7b**). Moreover, when using the light collector, the heated area in the center increases for higher temperatures, thus increasing the generated gradient.

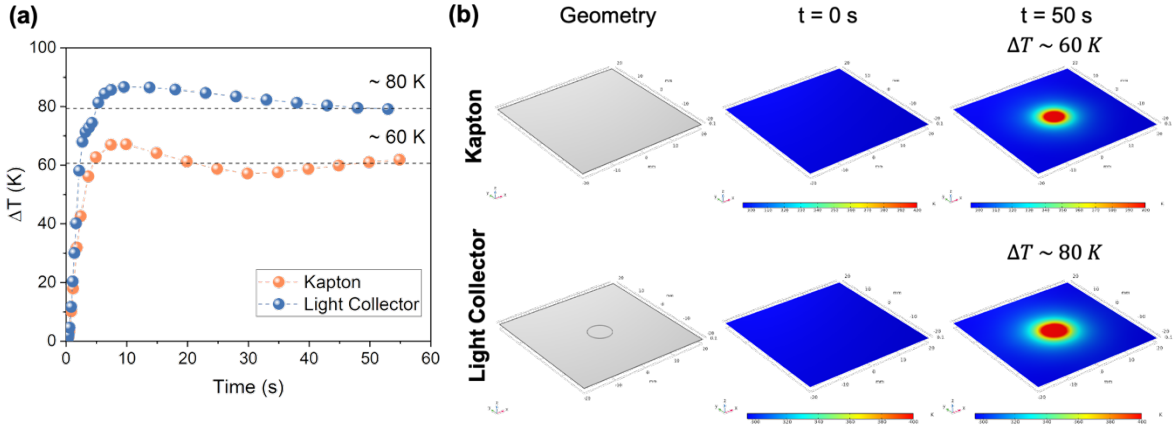

Figure 7 a) Simulated temperature gradients for the Kapton substrate and the light collector, with an incident gaussian laser beam of 2 W. The ΔT is calculated from the temperatures determined at 3.7 mm and 10. 5 mm from the center, corresponding to the length of a TE stripe in the developed device. b) Geometry and temperature distributions at t = 0 s and t = 50 s, for the Kapton substrate and the light collector (circle with radius = 3.5 mm), in a Kapton substrate.

2.2. Hybrid photothermoelectric device

Considering the aforementioned results, two radial flexible devices were produced with the presented TE ink, one with and another one without the light collector in the center to inspect its influence in the final performance of the PTE. The developed device comprises of 3 independent components (electric contacts, TE stripes, light collector), manufactured only by screen-printing (see **Figure 8a**). The chosen configuration allows the incidence of a laser beam in the center of the device, creating a temperature gradient from the inside to the outside (see **Figure 8b**). The devices are composed of 8 thermoelectric stripes, being a single mode device, *i.e.*, with only a p-type TE material.

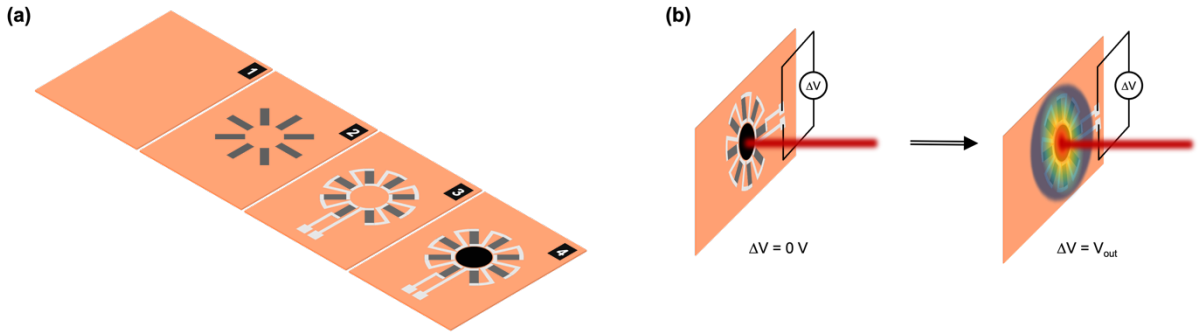

Figure 8 (a) Fabrication process by screen-printing of the photothermoelectric device: 1. Kapton substrate; 2. TE stripes; 3. Silver electric contacts; 4. Light collector made of carbon-based commercial ink. (b) Operation principle of the photothermoelectric device, where a laser beam is focused on the center of the device, creating a temperature gradient from the inside to the outside, generating a voltage between the terminals of the radial device.

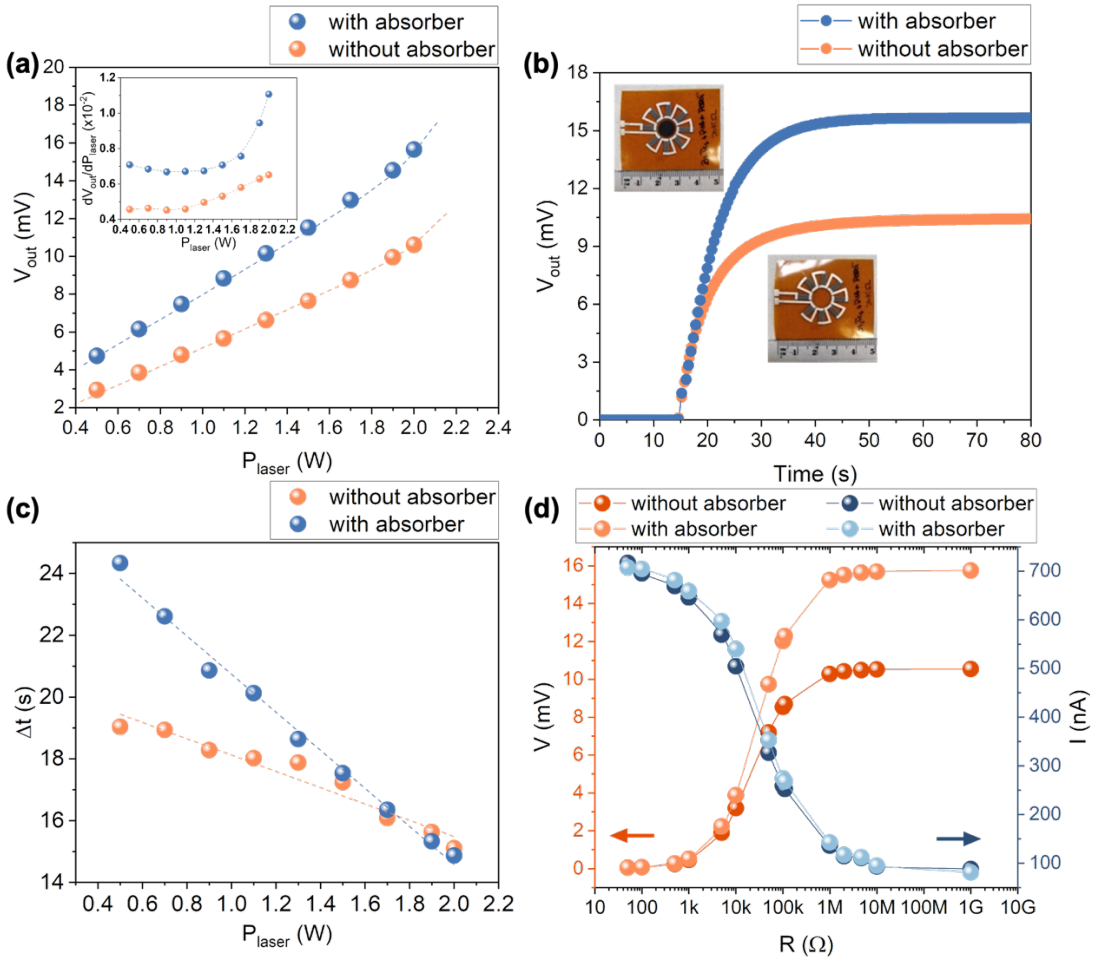

Figure 9 a) Device output voltage as a function of the laser power. Inset shows the first derivative of V_{out}, highlighting its nonlinearity. b) Response when the laser is turned on (P_{laser}=2W), for the devices without and with the light collector. c) Response times of the devices without and with the light collector, for different laser powers. d) Voltage and current generated by the two devices (without and with the light collector), as functions of probe resistance (P_{laser}=2W). Dashed lines are guides to the eyes.

The results of the device performance with a λ = 1450 nm and different laser powers, ranging from 0.5 W to 2 W (power density of 1.3 Wcm^{-2} and 2.6 Wcm^{-2}, respectively), and also for the specific case of P = 2 W, are summarized **Figure 9**.

Firstly, the open-circuit voltage (V_{out}) was measured for various applied laser powers (P_{laser}), as showed in **Figure 9a**. An apparent linear correlation can be observed, although looking at the first derivative (see inset in **Figure 9a**), an exponential increase is present for a threshold P_{laser}, that depends on the presence of the light collector. For this reason, this threshold is thought to be related to the flux of heat from the light absorption, leading to a non-linear temperature increase for P_{laser} higher than 1.1 W and 1.3 W without and with the light collector, respectively. The maximum achieved output voltages were ~ 11 mV and ~ 16 mV, without and with the light

collector, respectively. Moreover, it was observed that this output is maintained for 3 days with continuous illumination, with variations lower than 5 %. When compared with a similar radial device reported by Zhu *et al.*[7], the maximum output voltages appear lower, considering 8 TE stripes and a temperature gradient of 60 K (V_{out} ~ 66 mV). By choosing a TE ink with mechanical and electrical stability, the thermoelectric properties are inferior to the ones reported in a study with a similar composition [45]. Hence, if we consider their optimized Seebeck coefficient ($S \sim 144\ \mu V\ K^{-1}$), we can predict that the maximum output voltage that our device can reach would be ~ 69 mV, higher that the previously reported.

Besides the higher output, the response time is also influenced by the presence of the collector. As it can be seen in **Figure 9b**, when the laser is turned on, the device rapidly responds and reaches a stable V_{out} value. This response time decreases linearly with the increase of P_{laser} and tends to higher values with the implementation of the collector, particularly for lower powers of the laser (see **Figure 9c**). This can be explained by the different thermal conductivities of the collector and the substrate, causing different heat diffusions. Moreover, the developed device presents a low response time when compared with previous studies ($\Delta t < 30$ s)[7–9]. Secondly, through the characterization with a load resistance, the behaviors of voltage and current generated by the device were evaluated, as functions of that resistance (see **Figure 9d**). The results show that the presence of the light collector causes an increased voltage, as previously seen, but the generated current remains practically the same.

The maximum electrical current achieved was ~ 700 nA, a relatively low value due to the high electrical resistance of the device. By considering the determined electrical conductivity of the TE ink, the electrical resistance (R) of the device was calculated taking into account the shape factor and the series connected stripes, presenting a $R_{calculated}$ ~ 5 kΩ. Contrarily, the measured internal electrical resistance (R_{int} ~ 19 kΩ) shows a great discrepancy with the calculated value, caused by the high electrical resistance between the interfaces of the TE stripes with the electrical contacts, calculated to be ~ 875 Ω per interface.

Regarding the full electrical characterization, the devices seem to follow the predicted behavior, with a linear dependence between the current (I) and voltage (V), by the Ohm's law ($I = RV$), and a second-degree polynomial dependence of the power (P) with the voltage ($P = IV = V^2R$) (see **Figure 10**)[72].

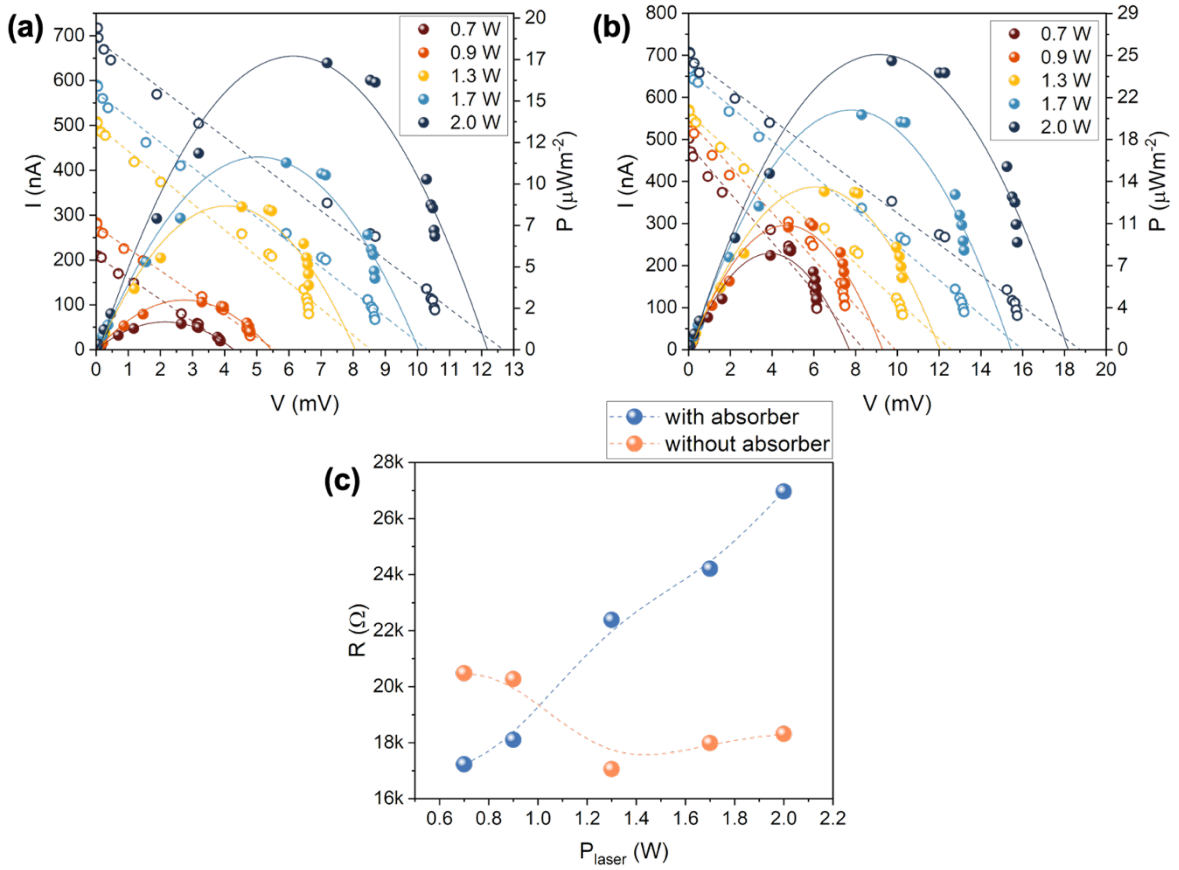

Figure 10 Full electrical characterization of the radial devices, i.e., generated voltage, current and power density, for different laser powers: a) without and b) with the light collector. c) Internal resistance determined by Ohm's Law (I=RV) for each laser power, without and with the light collector. Dashed and solid lines are visual cues.

As expected, the value of the output voltage increases with power of the incident laser, due to the increase of ΔT, for both cases. However, the values of current do not follow the same behaviour with the use of the light collector, as it can be seen by the maximum obtained values of I in **Figure 10b**. Taking into account Ohm's Law (I=RV), the changes in the current values arise from changes in the internal resistance (R_{int}) of the device, where an almost linear increase with the increase of P_{laser} can be seen for the device with the light collector, whereas the device without it has small variations (see **Figure 10c**). This can be explained by the high temperatures achieved at the extremities of the TE stripes (~ 400 K), at which the electrical conductivity of the TE material decreases in comparison to the value at room temperature, thus the R_{int} of the device increases.[73]

The maximum outputs were achieved by using a laser power of 2 W, but since a saturation is not observed, higher values are expected for even higher powers. The maximum generated

power densities obtained are ~ 17 μWm^{-2} and ~ 25 μWm^{-2}, without and with the light collector, respectively. As previously mentioned, the low power densities are due to the low thermoelectric efficiency of the TE ink. However, the improvement with the light collector is significant, *i.e.*, P_{max} increases almost by 50%. By using the value of the Seebeck coefficient of the TE ink (~ 33 μVK^{-1}), the created temperature gradient (ΔT) was calculated. Thus, for a laser power of 2 W, it was possible to achieve ΔT_{max} ~ 40 K and ΔT_{max} ~ 60 K, for the devices without and with the light collector, respectively. These values are in concordance with the ones obtained in the comparative thermal analysis of the substrate and the collector film.

Furthermore, bending tests were performed to the developed device to evaluate the effect of mechanical strain on the internal resistance of the device (see **Figure 11**). Similar to the results from the printed film, the variations of R_{int} presented values lower than 1% over more than 30 bending cycles, with a displacement of 10 nm. Moreover, for different bending angles, the average ΔR decreased linearly with the increasing bending angle, although the all the obtained values were lower than 0.2%. Hence, the device presents a similar mechanical response as the printed film, thus a mechanical strain will not compromise the performance of the device.

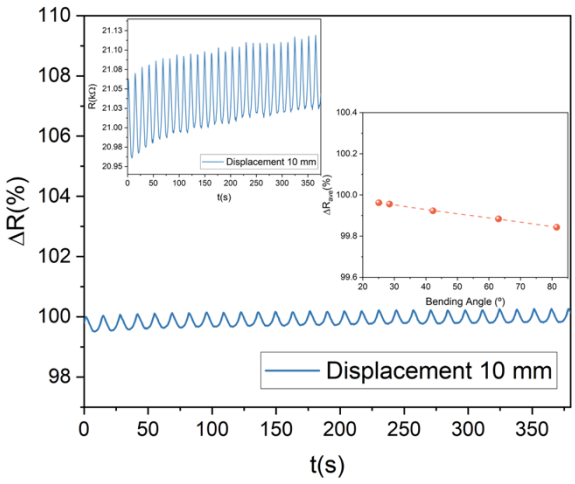

Figure 11 Bending test results, in particular the variation of R (ΔR (%)) during the measurement over 375 s, with a displacement of 10 mm. In inset on the left, the absolute value of R is presented over time during the test. In inset on the right, the average resistance variation (ΔRave (%)) is shown as a function of the bending angle, obtained for different displacement values.

2.3. Output under Extreme Conditions

Due to the specificity of the aerospace application of the developed device, mainly the CubeSat industry, the evaluation of the prototype performance under extreme conditions is essential. Therefore, the output voltage of the printed device was analyzed for a wide range of pressures (10^{-6} – 10^{3} Torr) and temperatures (180 – 300 K) (see **Figure 12**).

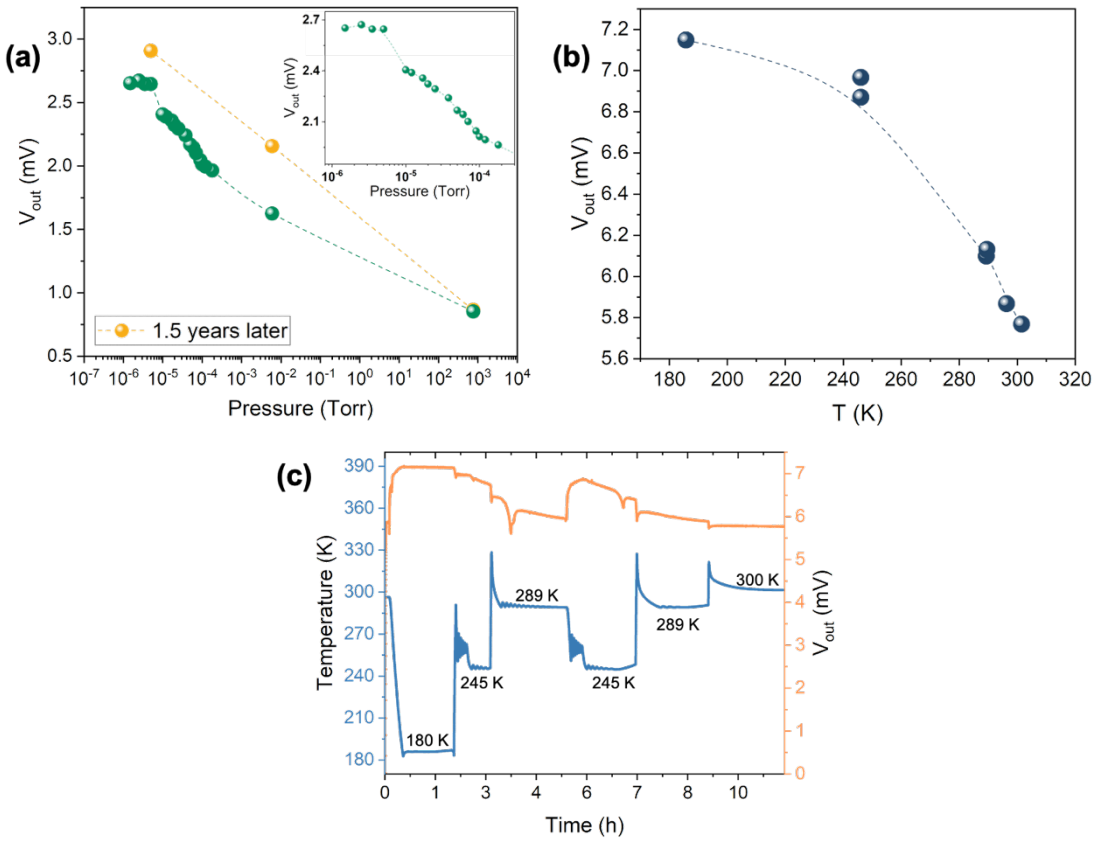

Figure 12 a) Output voltage as a function of the pressure inside the cryostat, and the results 1.5 years later. The inset shows the increase and later stabilization for lower pressures in higher vacuum. b) Output voltage of the radial TE device as a function of the temperature inside the chamber. c) Output voltage of the radial TE device and the controlled temperature measurement inside the chamber over a period of almost 12 h.

Both tests were performed with an incident laser beam power of 0.5 W. Looking into the influence of pressure on the efficiency of the prototype at room temperature, V_{out} generally increases with lower pressures, tending to stabilize for pressures lower than 10^{-5} Torr, as it can be seen in the inset graph in **Figure 12a**. The increase of the output voltage with lower pressures can be explained by two thermal phenomena, *i.e.*, the reduction of heat loss to the environment

and the enhancement of thermal contact. Regarding the first phenomenon, due to the lack of a propagation medium under vacuum, the heat loss through conduction and convection can be considered negligible, thus the reduced heat losses are only due to radiation.[74,75] As for the second phenomenon, the thermal contact of the overall system is seemingly enhanced by the reduction of air pockets present in the various interfaces (TE stripe – electrical contact; TE stripe – substrate; light collector – substrate), formed in the printing process.[76] Consequently, for lower pressures, the higher temperature gradient can be stablished, thus increasing the output voltage. Moreover, the results of the measurements performed 1.5 years later, reveal the reproducibility of the system, showing essentially the same variation and absolute values. Regarding the temperature tests (P ~ 10^{-6} Torr), the performance is enhanced for lower temperatures, expected due to the increase of the higher temperature gradient (see **Figure 12b**). However, for lower temperatures, this enhancement does not occur linearly with the temperature, which can be explained by the decreased temperature of the "hot side" that is not significant for higher temperatures. The low-temperature study was carried out during a period of almost 12h, taking into consideration the typical temperature changes that a CubeSat undergoes (245 – 289K)[77] (see **Figure 12c**). Besides the fact that the output of the device appears to be stable over time, it also presents a rapid response to the variations of the ambient temperature, which is therefore beneficial for those kinds of conditions. Overall, for low temperatures and low pressures, the output voltage increases by 25% and 230%, respectively.

3. Conclusions

In this work, a low-cost and flexible device based on the photothermoelectric effect was developed, appearing as a good candidate for long-distance wireless energy transfer and energy on demand at remote places, particularly for space exploration. The proposed prototype is composed of three independent parts (electric contacts, TE stripes, carbon-based light collector), all printed by screen-printing, for easy mass-production. The developed radial device can convert the light of an incident CW laser beam in its center into a temperature gradient, from the inside to the outside. The combination of a polymeric matrix (PEDOT:PSS + doped PVA) with inorganic microparticles ($Sb_{1.47}Bi_{0.53}Te_3$ + 1.77 atom % Bi) guaranteed flexible TE stripes, with mechanical properties and good thermoelectric conversion. With a laser beam at λ = 1450 nm and P = 2 W incident on the 8-stripe radial device, a maximum temperature gradient of ~ 60 K was achieved, leading to an output voltage of 16 mV and a maximum power density of 25 μWm^{-2}. The enhancement caused by the light collector was proven not only by the device's output, but also by thermal analysis directly in the material, and numerical simulations, showing

more than 30% of increase on the generated temperature gradient. Moreover, the viability of the proposed system at extreme conditions was verified, with an increase on the output voltage of 25% for low temperatures (T ~ 180 K) and 230% for low pressures (P ~ 10^{-6} Torr). In summary, the developed simple and low-cost radial flexible photothermoelectric device shows a great potential for the transfer of energy for low-power consumption electronics at remote places, regardless of environment conditions.

4. Experimental Section

TE powder preparation: Commercial SBT modules were used to produce the p-type thermoelectric powder. The modules were grinded with a mortar and pestle, to be reduced to powder. Then, a milling process was performed to homogenize of the particles' size, using a Retsch® planetary ball mill PM 100 with 250 rpm. In this system, 30 zirconia beads (1 cm of diameter) are the grinding media in a zirconia ball milling jar, where the particles were placed in a beads-to-powder mass ratio of 10:1, in an isopropanol medium. The milling process was was carried out in a 2-part process, i.e., 30 min of milling, followed 30 min of rest to prevent oxidation, repeated 3 times. The resulting powder was then sieved to obtain particles with dimensions lower than 50 μm.

Ink formulation and preparation: Two different polymers were used to for the polymeric matrix of the flexible thermoelectric ink, i.e., a non-conducive and a conductive. The non-conductive organic-polymer was produced using Polyvinyl alcohol - PVA (purchased from Sigma-Aldrich) doped with orthophosphoric acid - H_3PO_4 (85% analytical grade, purchased from Fisher Chemical) in 1:1 weight ratio. After the solubilization, the mixture of PVA-H_3PO_4 was incubated at 90 °C in a hot plate for 12 h, under continuous stirring, as reported by Pires and co-authors.[44] The conductive polymer Poly(3,4-ethylenedioxythiophene)-poly(styrenesulfonate) - PEDOT:PSS, was purchased from H. C. Stark, Inc (CleviosTM) and used after a continuous stirring, at 2000 rpm for 1h to ensure higher electrical conductivity. The PVA-H_3PO_4, the PEDOT:PSS, and the SBT powder were mixed until homogeneous, to formulate the thermoelectric ink, with a weight concentration of 16, 16, and 67 wt%, respectively. The obtained thermoelectric ink was used to print a screen pattern with 2 × 1.5 cm, and then dried at 130ºC for 10 min to obtain the flexible thermoelectric printed film. PI foil (DuPont, USA, thickness of 75 μm) was used as substrate, previously chemically treated with

10 wt% of KOH (for 60 min), 10 wt% of HCl aqueous solution (for 5 min) under continuous stirring, and then washed with Millipore water.[78] Additionally, commercial carbon-based ink, purchased from Elantas (Bectron® GP 9553VP), was used without further purification to print the light collector. The carbon-based ink thick film was printed in a pre-treated PI substrate using a screen pattern with 5 × 5 cm and then dried at 130ºC for 10 min. Commercial silver ink was purchased from VFP Ink Technologies and used as bought for the electrical contacts.

Characterization of TE/collector materials: The printed thermoelectric ink was characterized using a Scanning Electron Microscope (SEM), a Phillips-FEI/Quanta 400 FEG from the Materials Center of the University of Porto (CEMUP), with coupled X-ray Energy Dispersive Spectroscopy (EDS). The X-ray diffraction (XRD) measurements, in a Bragg-Brentano configuration, were performed on a SmartLab Rigaku diffractometer, at room temperature, with Cu Kα radiation (λ = 1.5406 Å, with a 200 mA, 45 kV), from 2θ = 10º to 100º. Regarding the transport properties, the room-temperature Seebeck coefficient was measured using an in-plane homemade setup composed of two independent Cu support pillars already reported in Pires *et al.*[44]. The room-temperature electrical conductivity of the printed thermoelectric film was measured using the four-point method where a 2410-C SourceMeter® from Keithley Instruments Inc. was used. The evaluation of the temperature dependence (20 K – 325 K) of S and σ of the TE film was carried out following Ferreira-Teixeira *et al.*[68] procedure.
Regarding the light collector, a UV-Vis-NIR Systems (Agilent Cary Spectrophotometer) was used to determine the absorption percentages with a scan rate of 600 nm/min, and a slit width of 2 nm. The 5 x 5 cm thick film was used to analyze the flexible collector and was measured from 200 nm to 2000 nm, with a spectral resolution of 1 nm. The absorption was determined by %Absorption=100%-%R-%T. The thickness of the printed films was measured using a Mitutoyo Digimatic Indicator.

Device Fabrication: Screen-printing were performed using a manual M-Print® machine. The three device parts were printed using three different mesh openings: 55 μm for the electrical contacts, 149 μm for the light collector, and 249 μm for the TE stripes. Firstly, the TE printed patterns were dried at 130 ºC for 10 min. Then, the electrical contacts were printed over the TE stripes, and then dried at 150 ºC for 10 min. Finally, a circular collector pattern was printed with the commercial carbon-based ink, and dried at 130 ºC during 10 min. The final TE stripes presented a length of 7 mm and a width of 2.5 mm. The electrical contacts presented a width of 1 mm. The circular light collector presented a diameter of 7 mm.

Prototype Testing: The performance of the devices was measured using commercial gold connectors with copper cables in a closed system inside a cryostat, at P ~ 10^{-6} Torr achieved by using a diffusion pump connected with a primary pump **Figure 13b**. The different temperatures (77 – 400 K) inside the cryostat were applied using liquid nitrogen (N_2) in the cooling structure of the system (second separate chamber), not being in contact with the device. A fiber laser with a wavelength of 1450 nm was used to generate different temperature gradients through different applied powers (0.5 – 2 W), with a spot of ~ 7 mm. The temperature control and measurement were performed using k-type thermocouples connected to a Lakeshore 336 Temperature Controller. The developed set-up can be seen in **Figure 13**.

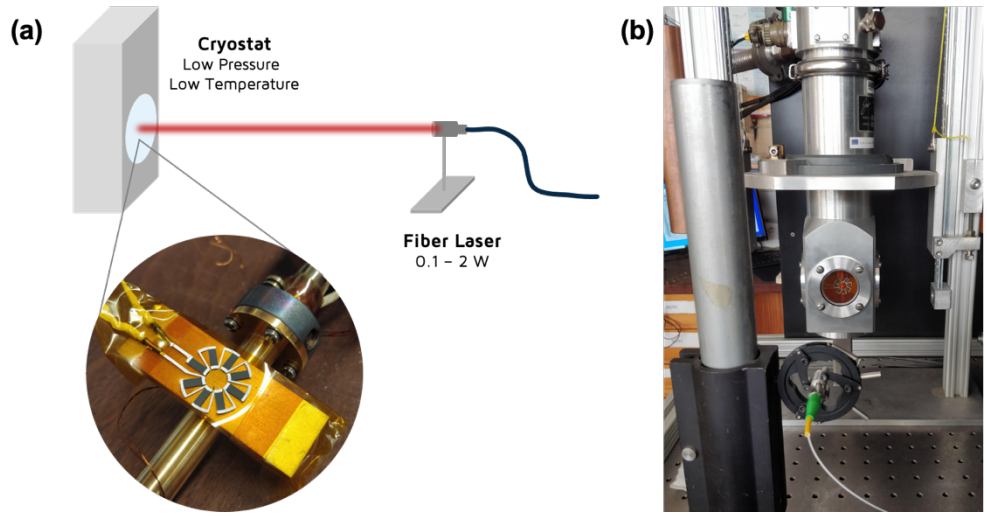

Figure 13 Developed set-up for the performance characterization of the fabricated prototype. (a) Schematic image of the concept of the set-up. (b) Image of the used cryostat and optical system.

In addition to the open-circuit output voltage measurement measured directly with nanovoltmeter, the device characterization was performed under a range of load resistances between 50 Ω and 1 GΩ with a fixed probe load (R = 50 Ω). Two different configurations were used for this end, *i.e.*, open and closed circuit, for voltage and current measurements, respectively. The voltage value was directly obtained, the current value was established by Ohm's law (I = V/R) with the probe load, and the power output was given by P = VI.

Supporting Information

Supporting Information is available from the Wiley Online Library or from the author.

Acknowledgements

This work was financially supported by Fundação para a Ciência e a Tecnologia (FCT)/MEC and FEDER under Program PT2020 through the projects UID/NAN/50024/2019, and NORTE-01-0145-FEDER022096 from NECL. The authors thank the funding from the European Union's Horizon 2020 research and innovation programme under grant agreement No 863307. Ref. H2020-FETOPEN-2018- 2019-2020-01. MMM is thankful to FCT for grant SFRH/BD/144229/ 2019. PR acknowledges the support of FCT for grant 2020.04562.BD.

Conflict of Interest

The authors declare no conflict of interest.

Received: ((will be filled in by the editorial staff))

Revised: ((will be filled in by the editorial staff))

Published online: ((will be filled in by the editorial staff))

References

[1] M. Song, P. Jayathurathnage, E. Zanganeh, M. Krasikova, P. Smirnov, P. Belov, P. Kapitanova, C. Simovski, S. Tretyakov, A. Krasnok, *Nat Electron* **2021**, *4*, 707.

[2] A. Ahmed, Z. Saadatnia, I. Hassan, Y. Zi, Y. Xi, X. He, J. Zu, Z. L. Wang, *Adv. Energy Mater.* **2017**, *7*, 1601705.

[3] K. Zhang, B. Ouyang, Y. Wang, Y. Xia, Y. Yang, *ACS Appl. Energy Mater.* **2019**, *2*, 7647.

[4] Y. Liu, X. Lan, J. Xu, W. Zhou, C. Liu, C. Liu, P. Liu, M. Li, F. Jiang, *ACS Appl. Mater. Interfaces* **2021**, *13*, 43155.

[5] D.-L. Wen, X. Liu, J.-F. Bao, G.-K. Li, T. Feng, F. Zhang, D. Liu, X.-S. Zhang, *ACS Appl. Mater. Interfaces* **2021**, *13*, 21401.

[6] Y. S. Jung, D. H. Jeong, S. B. Kang, F. Kim, M. H. Jeong, K.-S. Lee, J. S. Son, J. M. Baik, J.-S. Kim, K. J. Choi, *Nano Energy* **2017**, *40*, 663.

[7] W. Zhu, Y. Deng, M. Gao, Y. Wang, *Energy Conversion and Management* **2015**, *106*, 1192.

[8] Z. Guo, W. Zhu, Y. Yu, Y. Deng, *IEEE Electron Device Lett.* **2019**, *40*, 1832.

[9] M. He, Y.-J. Lin, C.-M. Chiu, W. Yang, B. Zhang, D. Yun, Y. Xie, Z.-H. Lin, *Nano Energy* **2018**, *49*, 588.

[10] C. Bianchi, A. C. Marques, R. C. da Silva, T. Calmeiro, I. Ferreira, *Sci Rep* **2021**, *11*, 24313.

[11] W. Kubo, M. Kondo, K. Miwa, *J. Phys. Chem. C* **2019**, *123*, 21670.

[12] X. Jin, H. Li, Y. Wang, Z. Yang, X. Qi, J. Yang, Y. Wang, *ACS Appl. Mater. Interfaces* **2022**, *14*, 27083.

[13] N. Sharma, J. Bar-David, N. Mazurski, U. Levy, *ACS Photonics* **2020**, *7*, 2468.

[14] J. Bai, Z. Pang, P. Shen, T. Chen, W. Shen, S. Wang, S. Chang, *Optics Communications* **2021**, *497*, 127184.
[15] P. Cheng, H. Wang, B. Müller, J. Müller, D. Wang, P. Schaaf, *ACS Appl. Mater. Interfaces* **2021**, *13*, 1818.
[16] W. Zhu, Y. Deng, L. Cao, *Nano Energy* **2017**, *34*, 463.
[17] S. Kim, Y. Na, C. Nam, C. K. Jeong, K. T. Kim, K.-I. Park, *Nano Energy* **2022**, *103*, 107824.
[18] C. Kim, M.-W. Jeong, S. Kim, S.-H. Oh, S.-Y. Lee, Y.-C. Joo, H. Shen, H. Lee, J. Yoon, Y. Joo, In *2020 IEEE 70th Electronic Components and Technology Conference (ECTC)*, IEEE, Orlando, FL, USA, **2020**, pp. 2242–2246.
[19] Z. Yuan, X. Tang, Z. Xu, J. Li, W. Chen, K. Liu, Y. Liu, Z. Zhang, *Applied Energy* **2018**, *225*, 746.
[20] B. Jabar, X. Qin, A. Mansoor, H. Ming, L. Huang, M. H. Danish, J. Zhang, D. Li, C. Zhu, H. Xin, C. Song, *Nano Energy* **2021**, *80*, 105512.
[21] K. Biswas, J. He, I. D. Blum, C.-I. Wu, T. P. Hogan, D. N. Seidman, V. P. Dravid, M. G. Kanatzidis, *Nature* **2012**, *489*, 414.
[22] W. Liu, D. Wang, Q. Liu, W. Zhou, Z. Shao, Z. Chen, *Adv. Energy Mater.* **2020**, *10*, 2000367.
[23] G.-H. Kim, L. Shao, K. Zhang, K. P. Pipe, *Nature Materials* **2013**, *12*, 719.
[24] N. Nandihalli, C.-J. Liu, T. Mori, *Nano Energy* **2020**, *78*, 105186.
[25] Q. Zhang, Y. Sun, W. Xu, D. Zhu, *Adv. Mater.* **2014**, *26*, 6829.
[26] J. Yang, H.-L. Yip, A. K.-Y. Jen, *Adv. Energy Mater.* **2013**, *3*, 549.
[27] D. Park, J. Kim, *Journal of the Korean Institute of Electrical and Electronic Material Engineers* **2022**, *35*, 203.
[28] E. Jin Bae, Y. Hun Kang, K.-S. Jang, S. Yun Cho, *Sci Rep* **2016**, *6*, 18805.
[29] T. Park, C. Park, B. Kim, H. Shin, E. Kim, *Energy Environ. Sci.* **2013**, *6*, 788.
[30] Y. Xu, Y. Jia, P. Liu, Q. Jiang, D. Hu, Y. Ma, *Chemical Engineering Journal* **2021**, *404*, 126552.
[31] Q. Yao, Q. Wang, L. Wang, L. Chen, *Energy Environ. Sci.* **2014**, *7*, 3801.
[32] H. J. Lee, G. Anoop, H. J. Lee, C. Kim, J.-W. Park, J. Choi, H. Kim, Y.-J. Kim, E. Lee, S.-G. Lee, Y.-M. Kim, J.-H. Lee, J. Y. Jo, *Energy Environ. Sci.* **2016**, *9*, 2806.
[33] Y. Wang, J. Yang, L. Wang, K. Du, Q. Yin, Q. Yin, *ACS Appl. Mater. Interfaces* **2017**, *9*, 20124.
[34] Z. Zhang, G. Chen, H. Wang, W. Zhai, *J. Mater. Chem. C* **2015**, *3*, 1649.
[35] C. Dun, C. A. Hewitt, H. Huang, J. Xu, D. S. Montgomery, W. Nie, Q. Jiang, D. L. Carroll, *ACS Appl. Mater. Interfaces* **2015**, *7*, 7054.
[36] C. Dun, C. A. Hewitt, H. Huang, J. Xu, C. Zhou, W. Huang, Y. Cui, W. Zhou, Q. Jiang, D. L. Carroll, *Nano Energy* **2015**, *18*, 306.
[37] W. Hou, X. Nie, W. Zhao, H. Zhou, X. Mu, W. Zhu, Q. Zhang, *Nano Energy* **2018**, *50*, 766.
[38] S. H. Kim, T. Min, J. W. Choi, S. H. Baek, J.-P. Choi, C. Aranas, *Energy* **2018**, *144*, 607.
[39] Z. Antar, J. F. Feller, H. Noël, P. Glouannec, K. Elleuch, *Materials Letters* **2012**, *67*, 210.
[40] J. Wang, H. Li, R. Liu, L. Li, Y.-H. Lin, C.-W. Nan, *Composites Science and Technology* **2018**, *157*, 1.
[41] Q. Meng, Y. Qiu, K. Cai, Y. Ding, M. Wang, H. Pu, Q. Yao, L. Chen, J. He, *ACS Appl. Mater. Interfaces* **2019**, *11*, 33254.
[42] C. Jiang, P. Wei, Y. Ding, K. Cai, L. Tong, Q. Gao, Y. Lu, W. Zhao, S. Chen, *Nano Energy* **2021**, *80*, 105488.
[43] A. G. El-Shamy, *Materials Science in Semiconductor Processing* **2019**, *100*, 245.

[44] A. L. Pires, I. F. Cruz, J. Silva, G. N. P. Oliveira, S. Ferreira-Teixeira, A. M. L. Lopes, J. P. Araújo, J. Fonseca, C. Pereira, A. M. Pereira, *ACS Applied Materials & Interfaces* **2019**, *11*, 8969.
[45] T. Zhang, K. Li, C. Li, S. Ma, H. H. Hng, L. Wei, *Adv. Electron. Mater.* **2017**, *3*, 1600554.
[46] X. Li, K. Cai, M. Gao, Y. Du, S. Shen, *Nano Energy* **2021**, *89*, 106309.
[47] N. A. Bhatti, M. H. Alizai, A. A. Syed, L. Mottola, *ACM Transactions on Sensor Networks* **2016**, *12*, 1.
[48] Z. Bi, T. Kan, C. C. Mi, Y. Zhang, Z. Zhao, G. A. Keoleian, *Applied Energy* **2016**, *179*, 413.
[49] S. Assawaworrarit, X. Yu, S. Fan, *Nature* **2017**, *546*, 387.
[50] C. Jiang, X. Li, S. W. M. Lian, Y. Ying, J. S. Ho, J. Ping, *ACS Nano* **2021**, *15*, 9328.
[51] T. D. Ponnimbaduge Perera, D. N. K. Jayakody, S. K. Sharma, S. Chatzinotas, J. Li, *IEEE Communications Surveys & Tutorials* **2018**, *20*, 264.
[52] A. Sahai, D. Graham, In *2011 International Conference on Space Optical Systems and Applications (ICSOS)*, IEEE, Santa Monica, CA, USA, **2011**, pp. 164–170.
[53] H. Suzuki, H. Yoshida, K. Kisara, T. Nakamura, M. Imaizumi, In *2014 IEEE 40th Photovoltaic Specialist Conference (PVSC)*, IEEE, Denver, CO, USA, **2014**, pp. 1834–1838.
[54] H. Chu, C. Wang, In *2020 International Conference on Optoelectronic Materials and Devices* (Eds.: Chen, S.; Wang, P.), SPIE, Guangzhou, China, **2021**, p. 2.
[55] G. A. Landis, *IEEE Aerospace and Electronic Systems Magazine* **1991**, *6*, 3.
[56] X. Lu, L. Sun, P. Jiang, X. Bao, *Adv. Mater.* **2019**, *31*, 1902044.
[57] X. Zhang, T.-T. Li, H.-T. Ren, H.-K. Peng, B.-C. Shiu, Y. Wang, C.-W. Lou, J.-H. Lin, *ACS Appl. Mater. Interfaces* **2020**, *12*, 55072.
[58] H. Park, D. Lee, G. Park, S. Park, S. Khan, J. Kim, W. Kim, *J. Phys. Energy* **2019**, *1*, 042001.
[59] H. Hemmati, A. Biswas, I. B. Djordjevic, *Proc. IEEE* **2011**, *99*, 2020.
[60] B. Jabar, A. Mansoor, Y. Chen, S. Jamil, S. Chen, G. Liang, F. Li, P. Fan, Z. Zheng, *Chemical Engineering Journal* **2022**, *435*, 135062.
[61] Z. Starý, J. Horák, M. Stordeur, M. Stölzer, *Journal of Physics and Chemistry of Solids* **1988**, *49*, 29.
[62] C. Chen, D.-W. Liu, B.-P. Zhang, J.-F. Li, *Journal of Elec Materi* **2011**, *40*, 942.
[63] J. Cardoso, O. GomezDaza, L. Ixtlilco, M. T. S. Nair, P. K. Nair, *Semicond. Sci. Technol.* **2001**, *16*, 123.
[64] T. Fang, X. Li, C. Hu, Q. Zhang, J. Yang, W. Zhang, X. Zhao, D. J. Singh, T. Zhu, *Adv. Funct. Mater.* **2019**, *29*, 1900677.
[65] O. Gh. Abdullah, S. B. Aziz, K. M. Omer, Y. M. Salih, *J Mater Sci: Mater Electron* **2015**, *26*, 5303.
[66] Q. Li, Z. Wei, Q. Ma, Z. Li, J. Luo, *ACS Omega* **2021**, *6*, 33883.
[67] J. Li, A. B. Huckleby, M. Zhang, *Journal of Materiomics* **2022**, *8*, 204.
[68] S. Ferreira-Teixeira, F. Carpinteiro, J. P. Araújo, J. B. Sousa, A. M. Pereira, *Review of Scientific Instruments* **2021**, *92*, 043904.
[69] E. Bilotti, O. Fenwick, B. C. Schroeder, M. Baxendale, P. Taroni-Junior, T. Degousée, Z. Liu, In *Comprehensive Composite Materials II*, Elsevier, **2018**, pp. 408–430.
[70] Y. Ueki, T. Aoki, K. Ueda, M. Shibahara, *International Journal of Heat and Mass Transfer* **2017**, *113*, 1130.
[71] G. Wypych, In *Databook of Antistatics*, Elsevier, **2014**, pp. 245–271.
[72] A. Montecucco, J. Siviter, A. R. Knox, *Applied Energy* **2015**, *149*, 248.
[73] O. Ben-Yehuda, R. Shuker, Y. Gelbstein, Z. Dashevsky, M. P. Dariel, *Journal of Applied Physics* **2007**, *101*, 113707.

[74] Q. Fu, Y. Xiong, W. Zhang, D. Xu, *Rev. Sci. Instrum.* **2017**, *88*, 095111.
[75] R. Bjørk, D. V. Christensen, D. Eriksen, N. Pryds, *International Journal of Thermal Sciences* **2014**, *85*, 12.
[76] B. Beltrán-Pitarch, J. García-Cañadas, *Vacuum* **2020**, *172*, 109088.
[77] A. Elhefnawy, A. Elmaihy, A. Elweteedy, *FME Transactions* **2021**, *49*, 1014.
[78] Park, Su-Jin, Lee, Eun-Jung, Kwon, Soo-Han, *Bulletin of the Korean Chemical Society* **2007**, *28*, 188.